



OPEN

Soft plasmons with stretchable spectroscopic response based on thermally patterned gold nanoparticles

Xinping Zhang, Jian Zhang, Hongmei Liu, Xueqiong Su & Li Wang

Institute of Information Photonics Technology and College of Applied Sciences, Beijing University of Technology, Beijing 100124, P. R. China.

SUBJECT AREAS:

NANOPHOTONICS AND
PLASMONICS

METAMATERIALS

Received
9 December 2013Accepted
7 February 2014Published
25 February 2014Correspondence and
requests for materials
should be addressed to
X.P.Z. (zhangxinping@
bjut.edu.cn)

Flexible photonic crystals are attractive devices owing to their multifold tunable parameters additionally introduced by soft substrates or by nanostructured, nano-doped, or nano-embedded soft matters. This not only extends significantly the intrinsic functions of photonic crystals, but also facilitates easy integration of the photonic crystal device into various optoelectronic and sensing systems. So far, flexible metallic photonic structures have been constructed on micrometer scales with complex fabrication procedures. Much simpler and more reproducible methods are expected to achieve such metamaterials in large scales and at low costs. In address to these challenges, we developed a straightforward approach to create soft plasmonic photonic crystals consisting of gold nanolines arranged on stretchable substrates with nanoscale periods, centimeter-scale areas, and high reproducibility using annealed gold nanoparticle colloids.

Flexible photonic crystals^{1–15} based on soft matters like polymers with response in different spectral bands may be applied extensively in optoelectronic devices, sensors, and tunable optical filters¹⁶. When active materials like polymeric semiconductors are incorporated into flexible photonic crystals, lasers or light-emitting devices with large tuning dynamics may be achieved^{17,18}. Photonic band gap structures consisting of self-assembled polystyrene nanoparticles have been used as a tunable Bragg mirror of a laser cavity¹⁹. Active photonic structures with periods of 30 μm have been achieved in luminescent organic films²⁰. Woodpile three-dimensional photonic crystals have been fabricated using polymers with nanocomposite doped with quantum dots as spontaneous emission device²¹.

Sensors for detecting different substances, different parameters, and different processes have been developed using photonic crystal structures. In particular, Fano coupling between plasmonic and photonic resonance modes was used to enhance the sensitivity significantly^{22–25}. Functions of sensors based on photonic structures may be largely extended or enhanced through flexibilization. Flexible photonic crystals based on self-assembled polymeric or dielectric spheres have been demonstrated for strain sensing applications²⁶. Three-dimensional polymeric photonic structures have been demonstrated for the optical properties that were tuned by pH values and temperatures²⁷. Silicon photonic devices have been fabricated on a flexible platform for strain sensing²⁸.

Various techniques have been demonstrated for achieving flexibilization of photonic crystal structures made of dielectric or metallic materials. Nanoimprinting is one of the most important approaches to achieved nano- or micro-scale photonic devices on flexible substrates^{1–3}. Soft photonic structures may be produced by nanoimprinting using hard stamp into soft matters⁶. Micro-transfer molding has been demonstrated for the fabrication of micrometer-scale polymeric photonic structures with optical response in the infrared⁷. Flexible films of photonic structures consisting of periodic porous multilayers have been produced for selective UV reflection⁸. A kind of photonic paper has been fabricated through self-assembly of silica-coated super-paramagnetic Fe_3O_4 nanoparticle colloids⁹. Stretchable photonic crystals of silicon nanowires embedded in a soft matrix have been reported with tunable optical response in the infrared¹⁰. Inorganic crystalline semiconductor nanomembranes have been transferred onto flexible substrates as Fano filters¹⁵.

Flexible metamaterials have been demonstrated with plasmonic microstructures arranged into two- (2D) or three-dimensional (3D) photonic crystals. Mechanically tunable plasmonic structures have been achieved by fabricating a monolayer array of metal-capped colloidal spheres on an elastomeric substrate²⁹. A flexible photonic device consisting of split ring resonators of Au or Ag have been produced on polymeric soft substrates for sensor applications¹¹. Thin-film photonic crystals based on superparamagnetic colloidal nanocrystal clusters with micrometer-scale periods have been reported with excellent mechanical bending properties¹². Large-area flexible

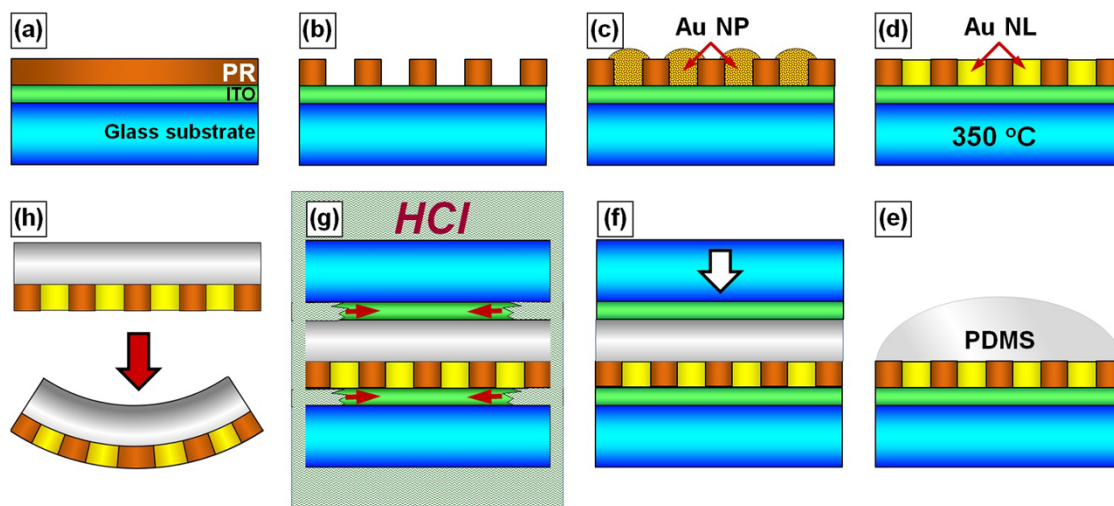


Figure 1 | Fabrication procedures of soft MPCs: (a) Spin-coating of photoresist (PR) onto the ITO glass substrate. (b) Fabrication of PR nano-grating structures using interference lithography. (c) Spin-coating of chemically synthesized gold nanoparticles (Au NP) in colloids with a concentration of 100 mg/ml in xylene. (d) Annealing the sample at 350 °C for 20 minutes to confine the gold into the grating grooves so that gratings of gold nanolines (Au NL) are produced interlaced with PR. (e) Spread PDMS on top of the MPC structures. (f) Another piece of ITO glass is placed to cover the PDMS-coated MPCs. (g) The sample is placed in HCl for 2 hours after the cross-linking polymerization process in an oven at 100 °C for 50 minutes, so that the ITO layers are sufficiently etched off. (h) The MPCs are transferred to PDMS and the soft MPCs are successfully lifted off the glass substrate.

3D optical negative index metamaterial was reported to be produced using a silicon stamp, blanket deposition of alternating layers of silver and magnesium fluoride, and subsequent transfer onto flexible substrates¹³. Photonic structures based on Silicon nanomembranes have been fabricated onto flexible substrates through stamp printing¹⁴. Soft lithography in combination electrodeposition has been demonstrated for the fabrication of woodpile structures of nickel with micrometer-scale periods³⁰. Micrometer-scale photonic structures of gold hemi-shells on self-assembled dielectric spheres have been produced on stretchable substrates³¹. Metamaterial films with micrometer-scale structures have been fabricated using roll-to-roll nanoimprinting process³².

However, flexible metamaterials with large effective areas, nano-scale periods, and plasmonic response in the visible spectrum have not been reported so far. In address to such nanofabrication challenges, we achieved flexible metallic photonic crystals (MPCs) with excellent stretchability and bendability by transferring thermally patterned MPCs consisting of gold nanolines with periods smaller than 400 nm to soft substrates. This defines a complete and defects-free fabrication technique with high success rate. The optical spectroscopic response defined by Fano resonance through plasmon-photonic coupling exhibits sensitive response and approximately linear tunability to the mechanical stretching on the soft substrates.

Discussion

Straightforward approaches are always expected in nanofabrications to achieve highly reproduced devices for practical applications. Large-scale flexible photonic crystals with optical response in the visible spectrum attract extensive interests in sensors and optoelectronic engineering, which post multifold challenges in the realization of practical devices or systems. In particular, metamaterials based on plasmonic-photonic coupling may be endowed with new functions through flexibilization. On the basis of such consideration, we developed a simple and practical approach for achieving flexible metallic photonic crystals (MPCs) consisting of gold nanolines arranged periodically on soft substrates with spectroscopic response in the visible spectrum.

MPCs are first fabricated on a hard glass substrate coated with an ITO layer. Then, multilayer structures of Glass/ITO/PDMS/MPC/ITO/Glass are created. After the ITO layers are etched off completely,

MPCs are transferred to the PDMS soft substrate, which defines a perfect liftoff process. The stretching/restoring experiments demonstrate excellent mechanical and spectroscopic flexibility of the soft MPCs, where plasmon resonance and its Fano coupling with the waveguide mode exhibits sensitive response to the mechanical actions on the structures. The resultant soft plasmonic structures are not only directly applicable as tunable photonic devices, but also important for strain, vibration, or displacement sensors.

The resultant flexible MPC nanodevice integrates the functions of plasmonic metamaterials and multifold tunability of soft-matter-based photonic devices. Efficient and defects-free fabrication, complete transfer from “hard” to “soft” substrates with 100% success rate constitute the unique features of this fabrication technique. Nano-scale periods, large effective area, strong Fano coupling through plasmonic-photonic interactions with excellent stretchable tunability constitute the advantages of the resultant device.

Methods

Figures 1(a)–(f) show schematically the fabrication procedures of the flexible MPCs. The initially hard substrate consists of a glass plate coated with a layer of indium tin oxide (ITO) as thick as 200 nm, which has an area of $20 \times 20 \text{ mm}^2$ and a thickness of 1 mm. S1805 photoresist from Rohm & Haas GmbH is spin-coated onto the ITO glass substrate at a speed of 2000 rpm for 30 s, as shown in Fig. 1(a). Interference lithography using a He-Cd laser at 325 nm produces a photoresist grating with a period easily adjustable from 200 to 800 nm by changing the separation angle between laser beams of the two interference arms, as shown in Fig. 1(b). Colloidal solution of chemically synthesized gold nanoparticles in xylene is spin-coated onto the top surface of the photoresist master grating, where the gold nanoparticles are in spherical shapes and have a mean diameter smaller than 5 nm. Based on different surface-energy properties of photoresist and ITO, gold nanoparticles with ligands are confined into the grating grooves³³, as shown in Fig. 1(c). Subsequent annealing process at 350 °C for about 20 minutes not only melts the gold nanoparticles and makes them fused together, but also enables further strong confinement of the gold into the grating grooves by the large surface tension of the molten gold³⁴. Thus, MPCs consisting of alternative gold/photoresist nanolines sitting on the ITO layer are produced after being cooled to room temperature, as shown in Fig. 1(d). Further characterizations of the annealing process are shown in Fig. S1 in the supporting information, where we show the SEM images of the MPC structures that are annealed at a temperature below 200 °C and above 350 °C in Fig. S1(a) and (b), respectively, to demonstrate the strong confinement of the gold into the grating grooves through the annealing processes.

In the transferring process, polydimethylsiloxane (PDMS) was used to produce the soft substrate, which has been applied extensively as stamps in nanoimprinting^{1–3,35}, directly in patterning photonic structures^{36,37}, in the fabrication of microfluidic device^{38,39}, and in the generation of structures spontaneously⁴⁰. PDMS is first spread on the top surface of the MPCs homogeneously with a thickness controllable from 1 to 3 mm after it is prepared by mixing the silicone gel with cross-linker at a volume



ratio of 10:1 and being processed in a vacuum chamber to remove the bubbles, as shown in Fig. 1(e). Then, another piece of ITO glass substrate is placed on the top of the spread PDMS with the ITO layer facing downward and touching the PDMS. A silicone rubber spacer with a thickness of about 1 mm (adjustable as expected) is placed between the two pieces of ITO glass. This top piece of ITO glass is then pressed down gently, so that a homogeneous layer of PDMS without observable defects or bubbles is produced between the two ITO glass substrates, as shown in Fig. 1(f). The top piece of ITO glass substrate is simply used to produce a smooth and flat surface, as well as a homogenous thickness of the resultant soft substrates. All of the above procedures have been performed under room temperature. The sample is then placed in an oven and heated to 100°C for about 50 minutes to achieve the cross-linking polymerization process. In the last stage, the dried sample is immersed in hydrochloric acid with a concentration of more than 20% for more than 60 minutes. The ITO layers on both substrates will be etched off through dissolving into the acid and the two substrates get removed automatically from the soft PDMS layer, as shown in Fig. 1(g). Thus, the MPCs are transferred to the soft PDMS substrate, as shown in Fig. 1(h). Cleaning process using pure water is necessary to remove the residues of hydrochloric acid and any other dirt produced in the above procedures.

Fig. 2(a), (b), and (c) show photographs of the flexible MPCs in different configurations. Fig. 2(a) and (b) demonstrate observations at different angles with consequently different diffraction colors for soft MPCs with periods of 650 and 400 nm, respectively. Bright and homogeneous colors over the effective areas on the MPCs not only imply successful transfer of the MPCs to the PDMS soft substrate, but also demonstrate strong photonic response of the devices. Fig. 2(c) shows different bending operations on the flexible MPCs, demonstrating excellent flexibility and strong tensile toughness of the soft-plasmon device. In particular, no defects have been observed on the MPC structures after the transfer process. This can be understood easily according to principles of this fabrication method, where no additional forces are needed to separate the PDMS soft layer from the hard substrates as long as the ITO layer has been etched off completely by the hydrochloric acid. Such a transferring process ensures complete transfer with 100% success rate, which constitutes one of the most important advantages of this technique.

Thus, the following features of the fabricated MPC structures on PDMS soft substrate can be concluded directly from the demonstration in Fig. 2: (1) Successful fabrication with efficient diffractions at different periods, as can be seen by the bright colors in Fig. 2(a) and (b) for $\Lambda = 650$ nm and $\Lambda = 400$ nm, respectively. (2) Excellent homogeneity of the fabricated structures in a centimeter-scale area with efficient diffraction over the whole structures. (3) Efficient operation over the broad visible spectral band with strong diffractions at different colors, where strong diffraction induces strong waveguide resonance modes and leads to strong Fano coupling. (4) Excellent bending performance of the MPCs on soft substrates, where large bending angles have been achieved without destroying the homogeneity, strong diffraction properties, and efficient operation over the visible spectral band illustrated by the strong diffractions of different colors.

Microscopic characterization. Figure 3 demonstrates microscopic characterization of the MPCs with a period of about 400 nm before and after the transferring

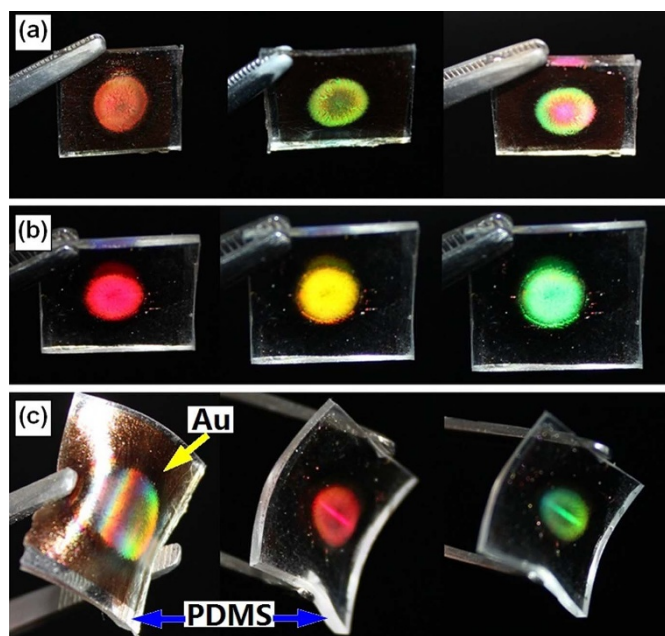


Figure 2 | Photographs of the resultant soft MPCs on PDMS at different observation angles so that the devices show different diffraction colors. (a) and (b): soft MPCs with a period of 650 and 400 nm, respectively. (c) Differently bended soft MPCs.

processes. Fig. 3(a) shows the scanning electron microscopic (SEM) images of the MPCs with a period of 400 nm on a glass substrate coated with 200-nm indium tin oxide (ITO) before they are transferred to soft substrates. The gold nanolines with a width of about 150 nm in average extend continuously and homogeneously in spite of very few occurrences of breaking-into-segments due to the annealing process³⁴. This implies a duty cycle of about 37.5% (width of gold nanolines over the grating period equals 150 nm/400 nm). This implies excellent confinement of gold into grooves of the template photoresist grating during the spin-coating and annealing processes. Although some smaller gold nanoparticles remain outside the dominant gold nanolines, they do not influence the global distribution of the plasmonic nano-line arrays and the optical performance, as will be shown in Fig. 4.

Fig. 3(b) shows the SEM image of the transferred MPCs consisting of gold nanolines on a PDMS soft substrate, where similarly continuous and homogeneous gold-nanolines can be observed. Due to the inductivity of both the PDMS substrate and the photoresist interlaced with the gold nanolines, it is difficult to obtain clear SEM images. This situation became even worse when we tried to perform high-resolution SEM measurements. A FEI Phenom desktop SEM system has been employed to perform the microscopic measurements on the transferred samples. It should be noted that the SEM image in Fig. 3(b) actually shows the bottom surface of the MPCs or the opposite surface of that shown in Fig. 3(a). Therefore, the small gold nanoparticles showing up in Fig. 3(a) are not observed in Fig. 3(b). Fig. 3(c) shows the atomic force microscopic (AFM) image, where a modulation depth of about 18 nm was measured. The strains from the flexible PDMS substrate affect differently on the gold nanolines and the in-between photoresist domains. Furthermore, the procedures presented in Fig. 1 show a schematic illustration with ideally designed composition of the grating structures consisting of alternatively arranged gold and photoresist nanolines. In practice, the thickness of gold is different from that of the photoresist and gaps may also exist between the gold and photoresist grating lines. These mechanisms led to modulations on the top surface of the MPCs transferred onto the PDMS substrate and explain the 18-nm height modulation. Both the SEM and AFM images in Fig. 3(b) and (c) verify excellent quality of the gold nanolines on soft substrates with large-scale homogeneity and continuity. Figure 3(b) and (c) actually present for the first time a direct observation of the topography on the bottom surface of the gold nanolines achieved through annealing the colloidal gold nanoparticles.

“Stretched” spectroscopic performance. In the optical spectroscopic characterizations, the MPC samples are mounted on a rotation stage in the horizontal plane with the gold nanolines of the MPCs standing vertically. However, for the MPCs on PDMS soft substrates, each end of the sample is firstly clamped on a separate translation stage, so that translation of either stage stretches the PDMS substrate horizontally. Then, the whole set is mount on the rotation stage. The rotation stage is used to change the incident angle in the horizontal plane. The re-collimated output beam from a halogen lamp is used as the white-light source and a USB 4000 spectrometer from Ocean Optics is used to measure the transmission spectra through the samples. Thus, the light is polarized horizontally and perpendicular to the gold nanolines for TM polarization and it is polarized vertically and parallel to the gold nanolines for TE polarization. The Fano resonance modes and the stretching sensor signals are measured as optical extinction spectra using different blank spectra. The optical spectroscopic performance of the flexible MPCs is as characterized in Fig. 4. For comparison, the optical extinction spectroscopic properties of the MPCs on “hard” substrates of ITO glass before the transfer process are first presented in Fig. 4(a), where the incident angle has been increased from 0 to 30 degrees. Since the Fano coupling between plasmon resonance of the gold nanolines and waveguide resonance mode is the most interesting mechanism to us for such MPC devices, only TM-polarization performance is shown in Fig. 4, where the polarization of the incident light is perpendicular to the gold nanolines and in the plane formed by the incident direction and the normal of the substrate. For MPCs on the “hard” substrates, the ITO layer functions as a waveguide and the Fano-like resonance induces enhanced transmission^{22,23}. The optical extinction spectrum has been calculated by $-\log_{10}(I_s/I_0)$, where I_s and I_0 denote the measured transmission spectra through the MPCs and the substrate, respectively. According to Fig. 4(a), plasmon resonance of the gold nanolines extends from 500 to 800 nm, while the waveguide resonance mode is located at about 630 nm for TM polarization. Therefore, the coupled mode is observed as a dip in the extinction spectrum center around 630 nm, which is split into two branches when light is incident at a non-zero angle ($\theta_i = 0 \sim 30^\circ$) and the degeneracy of the coupled mode is broken²². At normal incidence, the modulation “depth” of the coupled mode is as large as 0.5, corresponding to 70% optical extinction.

As the MPCs are transferred to PDMS soft substrates, no waveguide is available any more, where the top surface of the gold nanolines is now sitting on a bare PDMS substrate and the bottom is exposed to air. The corresponding spectroscopic response of this directly transferred device is shown in Fig. S2 in the supporting information, where the optical extinction spectra were measured for TM and TE polarizations, as shown in Fig. S2(a) and (b), respectively. Clearly, plasmon resonance is observed for TM polarization and is centered at about 666 nm by the extinction spectrum. Plasmon resonance is not clearly resolved for TE polarization. With tuning the angle of incidence, no Fano resonance is observed in Fig. S2, because no waveguide resonance mode is excited with no waveguide layer supplied with the device. The spectral shape of plasmon resonance is modified with increasing the angle of incidence, which is partially because of the slight shift of the light beam on the MPCs/PDMS sample and on the detection head of the spectrometer. To recover the coupled mode response of the MPCs, a layer of InGaZnO thinner than 50 nm is first deposited by pulsed laser deposition before a 200-nm layer of PMMA is spin-coated onto the structures, which

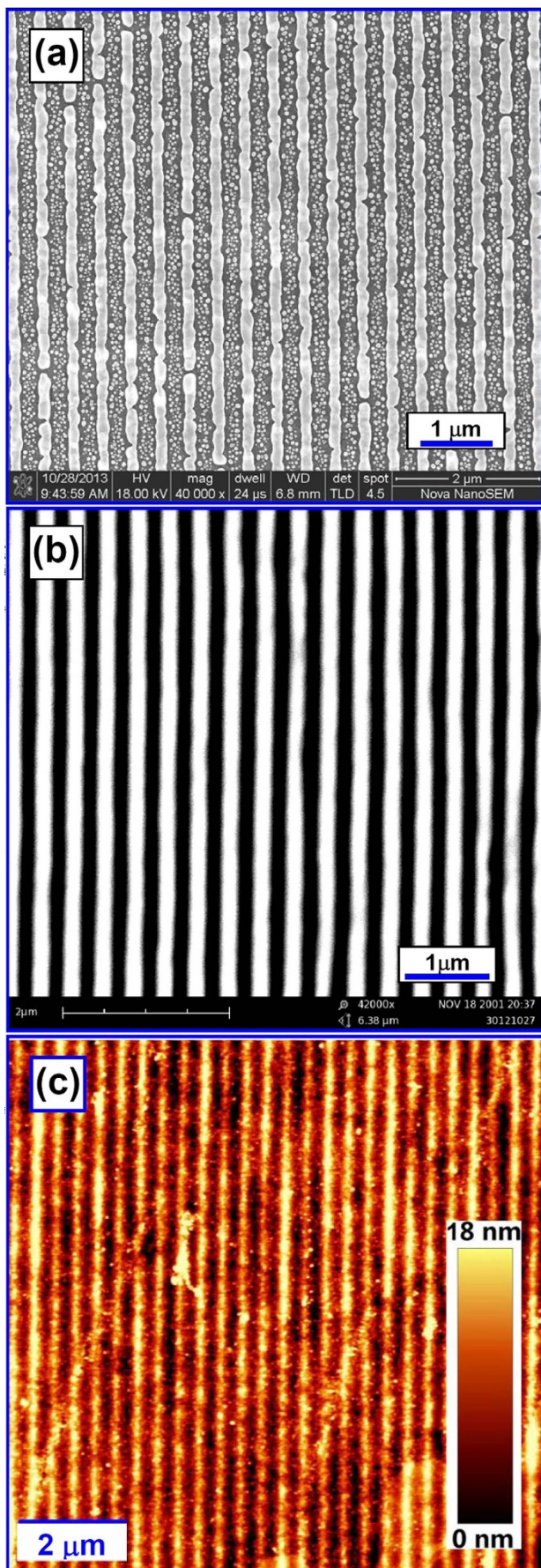


Figure 3 | Microscopic characterization of the MPCs: (a) SEM image of the MPCs on ITO glass hard substrates. (b) and (c): SEM and AFM images of the MPCs on the soft PDMS substrates, respectively.

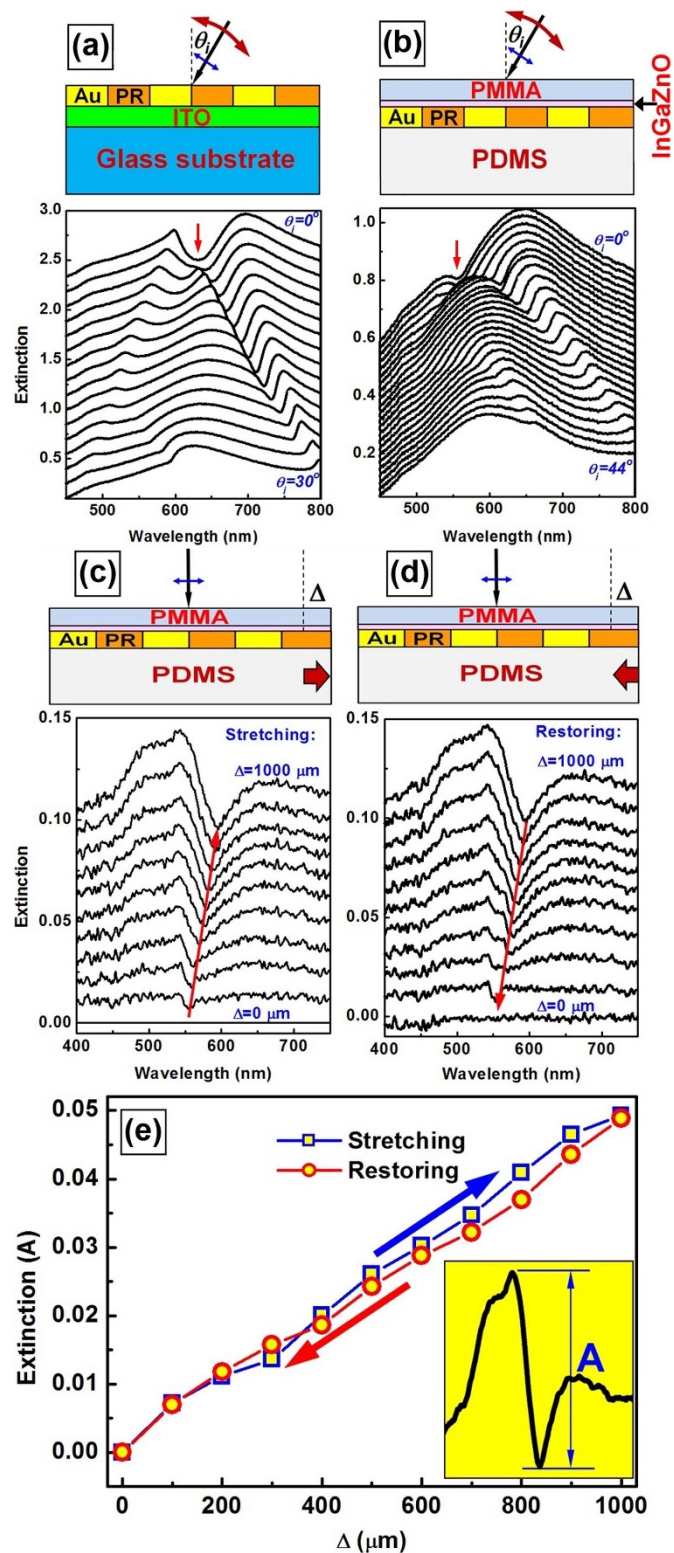


Figure 4 | Spectroscopic characterization of the MPCs. (a) and (b): angle-resolved tuning properties of optical extinction spectrum measured on the MPCs before and after the transferring processes, respectively, where the transmission spectrum in air is used as the blank and that through the MPCs as the signal. (c) and (d): Stretching and restoring experiments on the soft MPCs, respectively, where the transmission spectrum through the MPCs before stretching is used as the blank and those at different stretching amounts (Δ : 0 ~ 1000 μm) as the signals. (e) Variation of the sensing signal defined by the extinction amplitude (A) as a function of the stretching amount (Δ) plotted as the stretching and restoring traces.



functions as the new waveguide layer. The thin InGaZnO layer is used as an isolating layer to protect the PDMS from being damaged by the solvent of PMMA solution. Figure 4(b) shows the correspondingly measured optical extinction spectra as the incident angle (θ_i) of the light beam is increased from 0 to 44 degrees, where the transmission through the PDMS substrate is used as the blank. The Fano resonance resulting from the coupling between the waveguide and plasmon resonance mode is found blue-shifted from 630 nm to about 560 nm at normal incidence due to a complete change in the device configuration, as recognized by the “dips” in the optical extinction spectra and indicated by the downward arrows in Fig. 4(a) and (b). This is because the waveguide layer was changed from an ITO to a PMMA film and both the thickness and refractive index of the waveguide were changed accordingly, where the spectral position of Fano resonance is determined mainly by that of the waveguide resonance mode. The longer branch of the coupled mode is tuned to longer than 800 nm when the incident angle is larger than 44 degrees. The modulation depth of the coupled mode on the extinction spectra becomes much smaller, as compared with that in Fig. 4(a). The largest amplitude is reduced from 0.5 to less than 0.2. Plasmon resonance of the flexible gold nanolines is centered at about 600 nm, according to the spectrum at $\theta_i = 44^\circ$ with the waveguide mode tuned out of plasmon resonance.

Figure 4(c) and (d) demonstrate spectroscopic response of the flexible MPC device for stretching and restoring processes, respectively. The PDMS substrate has been clamped on either end edge to a translation stage with a separation distance of 10 mm and optical extinction spectra were measured as one of the stages is translated to stretch the substrate in steps of 100 μm . The measurements have been performed for TM polarization at normal incidence ($\theta_i = 0$). The transmission spectrum $I(\lambda, \Delta)$ through the flexible MPCs at an initial state ($\Delta = 0$) is used as the blank for both the stretching and the restoring experiments. Thus, the resultant signal spectrum is calculated by $-\log_{10}[I(\lambda, \Delta)/I(\lambda, 0)]$ and the amplitude of the signal is defined as the peak-to-valley difference (A) of the signal spectrum, as depicted in the inset of Fig. 4(e).

As the substrate is stretched, the most pronounced change is the enlargement of the grating period, which leads to the red shift of the waveguide resonance mode and consequently the red shift of Fano resonance, where the spectral position of Fano resonance is determined mainly by that of the waveguide resonance mode. Fig. 4(c) shows 10 optical extinction spectra for the stretching experiments, implying a total stretch amount of 1 mm or 10% the total length of the flexible substrate. The signal spectrum at $\Delta = 0$, a “zero” line is displayed since $I(\lambda, 0)$ has been used both as the signal and the blank transmission spectra. The amplitude of the signal spectrum (peak-to-valley difference: A) increases with increasing the stretching amount and is as large as 0.05 at $\Delta = 1000 \mu\text{m}$. A red-shift with increasing Δ is observed clearly with the dip feature of the signal spectrum, as marked by the red arrow in Fig. 4(c). This can be understood by looking at the measurement results in Fig. S3, where optical extinction spectra were measured for the stretching process with the transmission through a PDMS plate without MPC structures as the blank in the optical extinction calculation. Clearly, the Fano resonance recognized by small dips in the extinction spectra shifts to the red with increasing the stretching amount, as guided by the red arrow. However, in the sensor signals shown in Fig. 4(c) and 4(d), we used the transmission spectrum through the MPC structures at $\Delta = 0$ as the blank in the calculation of optical extinction, therefore, the sensor signal becomes stronger and red-shifted with increasing Δ . The above evolution dynamics reversed itself in the restoring process, as shown in Fig. 4(d). The shape and amplitude of the signal spectrum in Fig. 4(d) are basically consistent with those in Fig. 4(c), implying excellent reversibility. In particular, at $\Delta = 0$, no signal features can be observed. Thus, the device also shows excellent performance in returning to zero. Fig. 4(e) summarizes the variation of the signal amplitude (A) as a function of the stretching amount (Δ), the restoring trace basically repeats the stretching one with small deviations. The small mismatch between the two traces also results from the idle strokes of the translation stages. The stretching/restoring experiments in Fig. 4 have been repeated for 10 times without destroying the soft MPC structures or spectroscopic performance, which verifies excellent flexibility and toughness of the soft MPCs on PDMS substrates.

- Xia, Y. *et al.* Complex optical surfaces formed by replica molding against elastomeric masters. *Science* **273**, 347–349 (1996).
- Xia, Y. *et al.* Replica molding using polymeric materials: A practical step toward nanomanufacturing. *Adv. Mater.* **9**, 147–149 (1997).
- Gates, B. D. *et al.* New approaches to nanofabrication: molding, printing, and other techniques. *Chem. Rev.* **105**, 1171–1196 (2005).
- Vita, F., Lucchetta, D. E., Castagna, R., Criante, L. & Simoni, F. Large-area photonic structures in freestanding films. *Appl. Phys. Lett.* **91**, 103114 (2007).
- Jansen, C., Wietzke, S., Astley, V., Mittleman, D. M. & Koch, M. Mechanically flexible polymeric compound one-dimensional photonic crystals for terahertz frequencies. *Appl. Phys. Lett.* **96**, 111108 (2010).
- Park, J. *et al.* Conformable solid-index phase masks composed of high-aspect-ratio micropillar arrays and their application to 3D nanopatterning. *Adv. Mater.* **23**, 860–864 (2011).
- Smith, D. *et al.* Perfluorocyclobutyl copolymers for microphonics. *Adv. Mater.* **14**, 1585–1589 (2002).
- Castro Smirnov, J. R., Calvo, M. E. & Míguez, H. Selective UV reflecting mirrors based on nanoparticle multilayers. *Adv. Funct. Mater.* **23**, 2805–2811 (2013).
- Ge, J., Goebel, J., He, L., Lu, Z. & Yin, Y. Rewritable photonic paper with hygroscopic salt solution as ink. *Adv. Mater.* **21**, 4259–4264 (2009).
- Yu, C. L. *et al.* Stretchable photonic crystal cavity with wide frequency tunability. *Nano Lett.* **13**, 248–252 (2013).

- Xu, X. L. *et al.* Flexible visible-infrared metamaterials and their applications in highly sensitive chemical and biological sensing. *Nano Lett.* **11**, 3232–3238 (2011).
- Kim, H. *et al.* Structural colour printing using a magnetically tunable and lithographically fixable photonic crystal. *Nat. Photon.* **3**, 534–540 (2009).
- Chanda, D. *et al.* Large-area flexible 3D optical negative index metamaterial formed by nanotransfer printing. *Nat. Nanotechnol.* **6**, 402–407 (2011).
- Xu, X. *et al.* Stamp printing of silicon-nanomembrane-based photonic devices onto flexible substrates with a suspended configuration. *Opt. Lett.* **37**, 1020–1022 (2012).
- Zhou, W. *et al.* Flexible photonic-crystal Fano filters based on transferred semiconductor nanomembranes. *J. Phys. D: Appl. Phys.* **42**, 234007 (2009).
- Zeng, B., Gao, Y. & Bartoli, F. J. Ultrathin nanostructured metals for highly transmissive plasmonic subtractive color filters. *Sci. Rep.* **3**, 2840; doi:10.1038/srep02840 (2013).
- Riechel, S. *et al.* A nearly diffraction limited surface emitting conjugated polymer laser utilizing a two-dimensional photonic band structure. *Appl. Phys. Lett.* **77**, 2310 (2000).
- Lu, T.-W., Chiu, L.-H., Lin, P.-T. & Lee, P.-T. One-dimensional photonic crystal nanobeam lasers on a flexible substrate. *Appl. Phys. Lett.* **99**, 071101 (2011).
- Lawrence, J. R., Ying, Y., Jiang, P. & Foulger, S. H. Dynamic tuning of organic lasers with colloidal crystals. *Adv. Mater.* **18**, 300–303 (2006).
- Aparicio, F. J. *et al.* Transparent nanometric organic luminescent films as UV-active components in photonic structures. *Adv. Mater.* **23**, 761–765 (2011).
- Ventura, M. J. & Gu, M. Engineering spontaneous emission in a quantum-dot-doped polymer nanocomposite with three-dimensional photonic crystals. *Adv. Mater.* **20**, 1329–1332 (2008).
- Christ, A., Tikhodeev, S. G., Gippius, N. A., Kuhl, J. & Giessen, H. Waveguide-plasmon polaritons: strong coupling of photonic and electronic resonances in a metallic photonic crystal slab. *Phys. Rev. Lett.* **91**, 183901 (2003).
- Luk'yanchuk, B. *et al.* The Fano resonance in plasmonic nanostructures and metamaterials. *Nat. Mater.* **9**, 707–715 (2010).
- Zhang, X. P., Ma, X. M., Dou, F., Zhao, P. X. & Liu, H. M. A biosensor based on metallic photonic crystals for the detection of specific bioreactions. *Adv. Funct. Mater.* **21**, 4219–4227 (2011).
- Väkeväinen, A. I. *et al.* Plasmonic surface lattice resonances at the strong coupling regime. *Nano Lett.* DOI: 10.1021/nl4035219 (2014).
- Pursiainen, O. L. J. *et al.* Compact strain-sensitive flexible photonic crystals for sensors. *Appl. Phys. Lett.* **87**, 101902 (2005).
- Honda, M., Seki, T. & Takeoka, Y. Dual tuning of the photonic band-gap structure in soft photonic crystals. *Adv. Mater.* **21**, 1801–1804 (2009).
- Fan, L. *et al.* Direct fabrication of silicon photonic devices on a flexible platform and its application for strain sensing. *Opt. Express* **20**, 20564–20575 (2012).
- Zhu, X., Shi, L., Liu, X., Zi, J. & Wang, Z. A mechanically tunable plasmonic structure composed of a monolayer array of metal-capped colloidal spheres on an elastomeric substrate. *Nano Res.* **3**, 807 (2010).
- Lee, J.-H., Kim, Y.-S., Constant, K. & Ho, K.-M. Woodpile metallic photonic crystals fabricated by using soft lithography for tailored thermal emission. *Adv. Mater.* **19**, 791–794 (2007).
- Zhu, X. *et al.* A stretch-tunable plasmonic structure with a polarization-dependent response. *Opt. Express* **20**, 5237–5242 (2012).
- Ok, J. G. *et al.* Continuous and scalable fabrication of flexible metamaterial films via roll-to-roll nanoimprint process for broadband plasmonic infrared filters. *Appl. Phys. Lett.* **101**, 223102 (2012).
- Zhang, X. P. *et al.* Metallic photonic crystals based on solution-processible gold nanoparticles. *Nano Lett.* **6**, 651–655 (2006).
- Zhang, X. P. *et al.* Large-area two-dimensional photonic crystals of metallic nanocylinders based on colloidal gold nanoparticles. *Appl. Phys. Lett.* **90**, 133114 (2007).
- Gargas, D. J., Muresan, O., Sirbully, D. J. & Buratto, S. K. Micropatterned porous-silicon Bragg mirrors by dry-removal soft lithography. *Adv. Mater.* **18**, 3164–3168 (2006).
- Wu, D. *et al.* Curvature-driven reversible in situ switching between pinned and roll-down superhydrophobic states for water droplet transportation. *Adv. Mater.* **23**, 545–549 (2011).
- Son, J. G., Hannon, A. F., Gotrik, K. W., Alexander-Katz, A. & Ross, C. A. Hierarchical nanostructures by sequential self-assembly of styrene-dimethylsiloxane block copolymers of different periods. *Adv. Mater.* **23**, 634–639 (2011).
- Quinto-Su, P. A. *et al.* Examination of laser microbeam cell lysis in a PDMS microfluidic channel using time-resolved imaging. *Lab Chip* **8**, 408–414 (2008).
- Palleau, E., Reece, S., Desai, S. C., Smith, M. E. & Dickey, M. D. Self-healing stretchable wires for reconfigurable circuit wiring and 3D microfluidics. *Adv. Mater.* **25**, 1589–1592 (2013).
- Bowden, N., Brittain, S., Evans, A. G., Hutchinson, J. W. & Whitesides, G. M. Spontaneous formation of ordered structures in thin films of metals supported on an elastomeric polymer. *Nature* **393**, 146–149 (1998).

Acknowledgments

We acknowledge the 973 program (2013CB922404) and the National Natural Science Foundation of China (11274031) for the support, Prof. B. Sun from Soochow University for the fruitful discussions.



Author contributions

X.P.Z. designed this research work and all the experiments, performed the fabrication procedures, spectroscopic measurements, and data analysis, and wrote the paper. J.Z. measured the AFM and SEM images. H.M.L. synthesized the gold nanoparticles. X.Q.S. and L.W. prepared the InGaZnO spacer layer using pulsed laser deposition. All authors reviewed the manuscript.

Additional information

Supplementary information accompanies this paper at <http://www.nature.com/scientificreports>

Competing financial interests: The authors declare no competing financial interests.

How to cite this article: Zhang, X.P., Zhang, J., Liu, H.M., Su, X.Q. & Wang, L. Soft plasmons with stretchable spectroscopic response based on thermally patterned gold nanoparticles. *Sci. Rep.* **4**, 4182; DOI:10.1038/srep04182 (2014).



This work is licensed under a Creative Commons Attribution-NonCommercial-ShareAlike 3.0 Unported license. To view a copy of this license, visit <http://creativecommons.org/licenses/by-nc-sa/3.0>